Electronic Supplementary Material (ESI) for Catalysis Science & Technology.

Supporting Information

Iodide ions as invisible chemical scissors tailoring carbon nitride for highly-efficient photocatalytic H_2O_2 evolution

Dawei Yu†, Weiran Gong†, Xinyu Zhi†, Yang Wu, Xin Gao, Huinan Che*, Yanhui Ao

Key Laboratory of Integrated Regulation and Resource Development on Shallow Lakes, Ministry of Education, College of Environment, Hohai University, No.1, Xikang road, Nanjing, 210098, China

†These authors contributed equally to this work.

**Corresponding author. E-mail: chehuinan@hhu.edu.cn (H. Che)*

Figure S1. (a) Standard curves for different concentration of H_2O_2 and (b) The linear relationship of concentration of H_2O_2 vs. UV-vis absorption intensity.

Figure S2. XPS survey spectra of BCN, TCN, BCN/$NaI_{0.4}$ and TCN/$NaI_{0.4}$.

Figure S3. XPS spectra I 3d for TCN/$NaI_{0.4}$.

Figure S4. (a-b) Typical AFM images and the height profile along the line in AFM of TCN/$NaI_{0.4}$.

Figure S5. Histogram of H_2O_2 production for BCN, TCN, BCN/$NaI_{0.4}$ and TCN/$NaI_{0.4}$.

Figure S6. Time profiles of H_2O_2 production for TCN/$NaI_{0.4}$, TCN/$NaI_{0.3}$, TCN/$NaI_{0.1}$ under visible light irradiation.

Figure S7. UV–vis absorption spectra of H_2O_2 produced with IPA in photocatalytic stage of (a) BCN and (b) TCN at different times.

Figure S8. UV–vis absorption spectra of H_2O_2 produced with IPA in photocatalytic stage of (a) BCN/$NaI_{0.4}$ and (b) TCN/$NaI_{0.4}$ at different times.

Figure S9. Photocatalytic H_2O_2 production activity of TCN/$NaI_{0.4}$ under different conditions.

Figure S10. Photocatalytic H_2O_2 production activity of TCN/$NaI_{0.4}$ under 420 nm, 500 nm, 550 nm light irradiation.

Figure S11. Histogram of H_2O_2 production for TCN/$NaI_{0.4}$ under 420 nm, 500 nm, 550 nm light irradiation.

Figure S12. Isosurface map of IRI of pure BCN and TCN/NaI.

Figure S13. Total density of states (DOS) and partial density of states (PDOS) of pure BCN and TCN/NaI.

Figure S14. Electronic structure of the optimized HOMO and LUMO of pure BCN. Green and blue isosurfaces represent electron and hole distributions, respectively. The isosurface value is 0.003 e/$Å^3$.

Figure S15. Electronic structure of the optimized HOMO and LUMO of O_2 adsorbed BCN. Green and blue isosurfaces represent electron and hole distributions, respectively. The isosurface value is 0.003 e/$Å^3$.

Figure S16. Electronic structure of the optimized HOMO and LUMO of TCN/NaI. Green and blue isosurfaces represent electron and hole distributions, respectively. The isosurface value is 0.003 e/Å^3.

Figure S17. Electronic structure of the optimized HOMO and LUMO of O_2 adsorbed TCN/NaI. Green and blue isosurfaces represent electron and hole distributions, respectively. The isosurface value is 0.003 e/Å^3.

Experimental sections

Characterization

In this experiment, in order to determine the microscopic morphology of the catalysts, scanning electron microcopy (SEM; S-4800, Hitachi, Japan) and transmission electron microscope (TEM; JEM-F200, JEOL, Japan) were put into effect. The powder X-ray diffraction (XRD; Rigaku, Japan) was used to analyze the crystalline phase structure of sample. Additionally, in order to further explore the chemical structure of the catalysts, the X-ray photoelectron spectroscopy (XPS; Thermo- Scientific K-Alpha+, USA) and fourier-transform infrared spectroscopy (FTIR; Tensor 27, Bruker Optics, German) were performed. By using the UV-Vis spectrophotometer (UV-3600, Shimadzu, Japan) with a reflectance standard $BaSO_4$ powder, UV–vis diffuse reflectance spectra (DRS) was obtained. Fluorescence spectrometer (F-7000, Hitachi, Japan) was used to carried out the photoluminescence (PL) spectroscopy with 370 nm excitation wavelength. Electron spin resonance (ESR) experiments were performed on the Bruker ESR JESFA200 spectrometer.

DFT calculation

The geometry optimization and excited-state calculations was performed by PBE0-D3(BJ) exchange-correlation functional with the 6-311G(d) basis set based on Gaussian 16 C.01 code.[1-6] Frequency calculations were performed to ensure that the stability configuration has no imaginary frequency. The solvent effect of H_2O was considered using self-consistent reaction field (SCRF) based on the solvation model density (SMD) implicit solvent model.[7] Frontier molecular orbital, Fukui function,[8-10] density of states (DOS), interaction region indicator (IRI),[11] hole-electron analysis[12] and interfragment charge transfer (IFCT) were calculated with Multiwfn 3.8(dev).[13] All structures and isosurfaces images were visualized by VMD 1.9.3.[14]

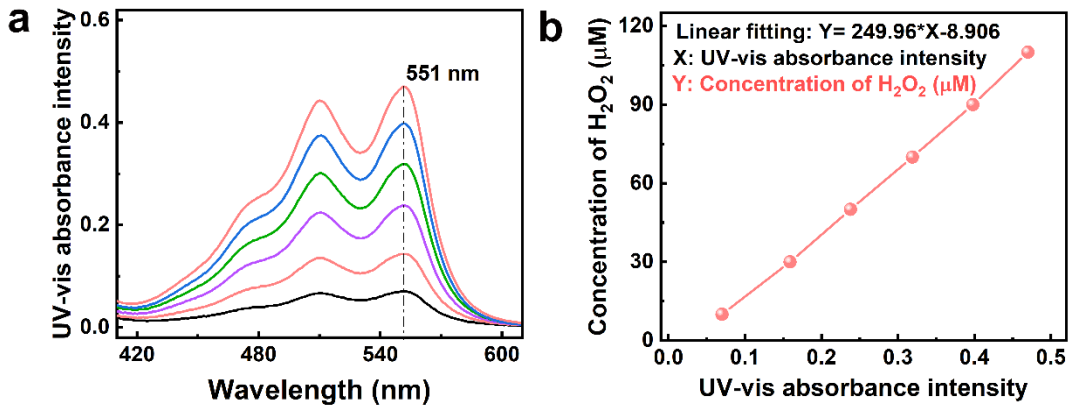

Figure S1. (a) Standard curves for different concentration of H_2O_2 and (b) The linear relationship of concentration of H_2O_2 vs. UV-vis absorption intensity.

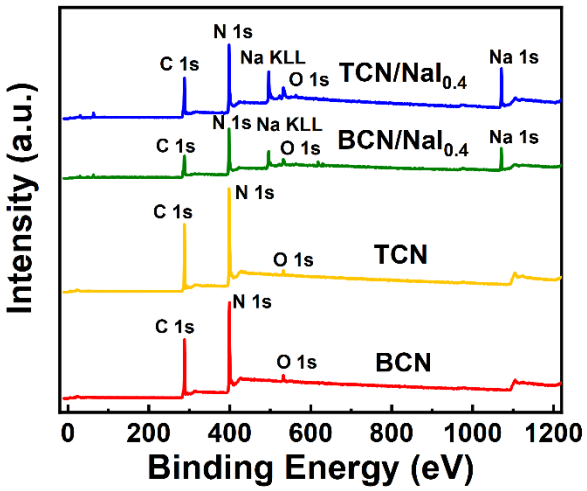

Figure S2. XPS survey spectra of BCN, TCN, BCN/$NaI_{0.4}$ and TCN/$NaI_{0.4}$.

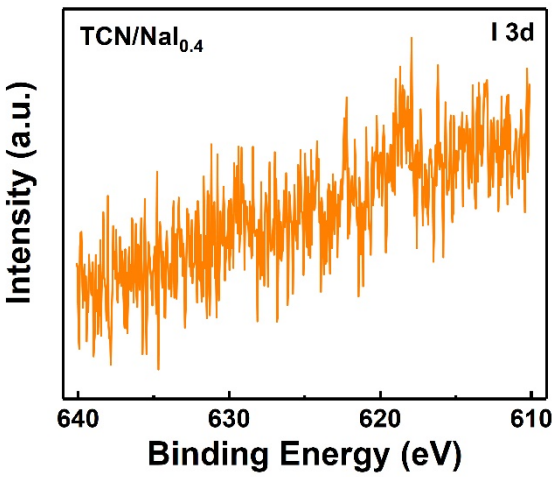

Figure S3. XPS spectra I 3d for TCN/$NaI_{0.4}$.

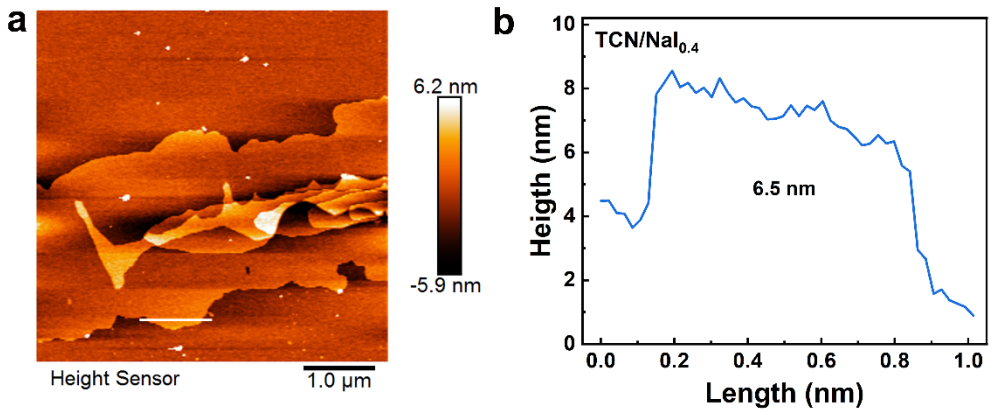

Fig. S4 (a-b) Typical AFM images and the height profile along the line in AFM of $TCN/NaI_{0.4}$.

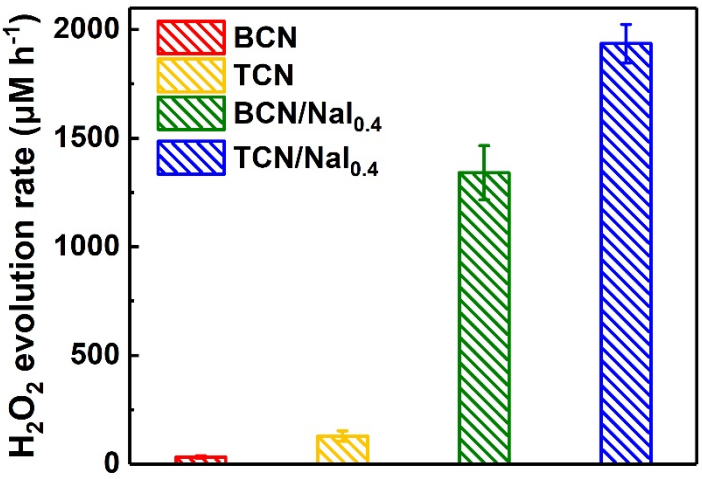

Figure S5. Histogram of H_2O_2 production for BCN, TCN, BCN/$NaI_{0.4}$ and TCN/$NaI_{0.4}$.

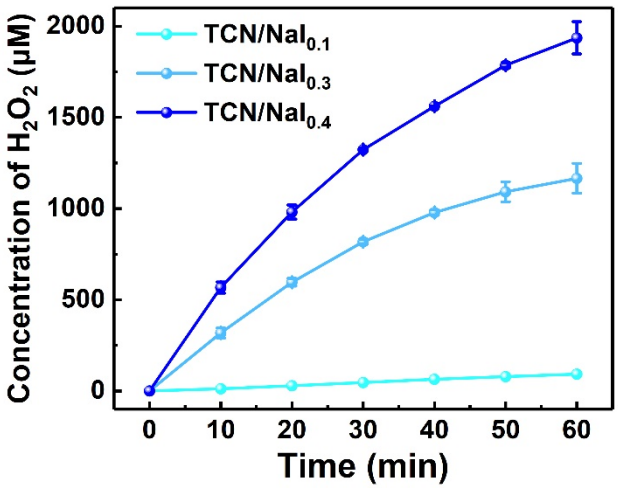

Figure S6. Time profiles of H_2O_2 production for TCN/NaI$_{0.4}$, TCN/NaI$_{0.3}$, TCN/NaI$_{0.1}$ under visible light irradiation.

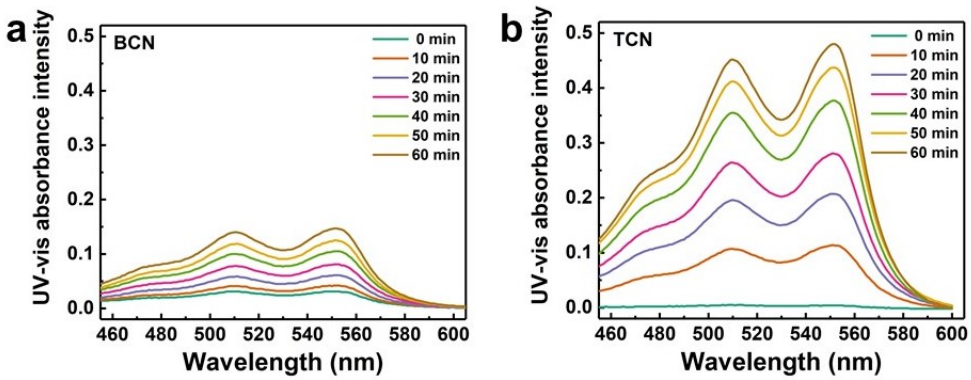

Figure S7. UV–vis absorption spectra of H_2O_2 produced with IPA in photocatalytic stage of (a) BCN and (b) TCN at different times.

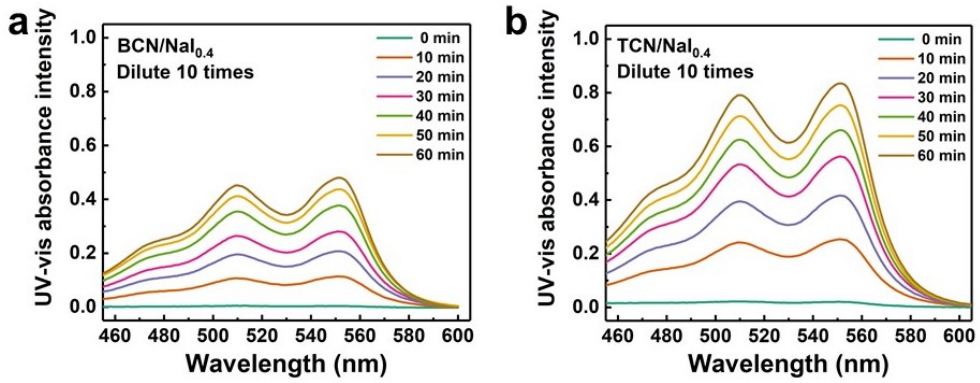

Figure S8. UV–vis absorption spectra of H_2O_2 produced with IPA in photocatalytic stage of (a) BCN/$NaI_{0.4}$ and (b) TCN/$NaI_{0.4}$ at different times.

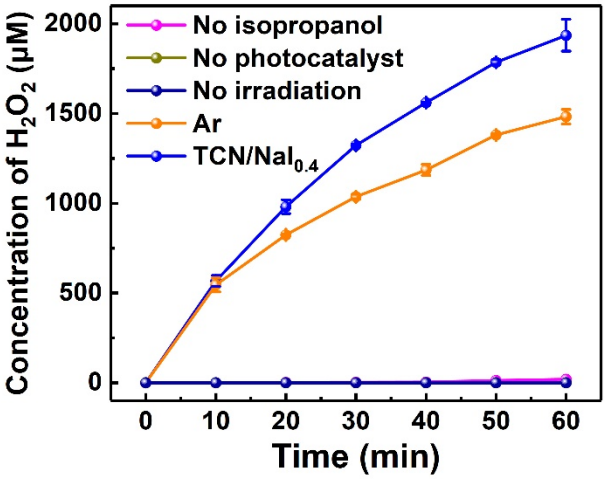

Figure S9. Photocatalytic H_2O_2 production activity of TCN/$NaI_{0.4}$ under different conditions.

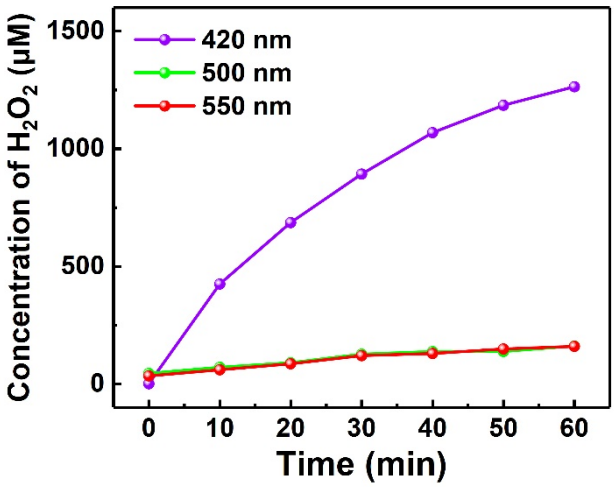

Figure S10. Photocatalytic H_2O_2 production activity of TCN/$NaI_{0.4}$ under 420nm, 500nm, 550nm light irradiation.

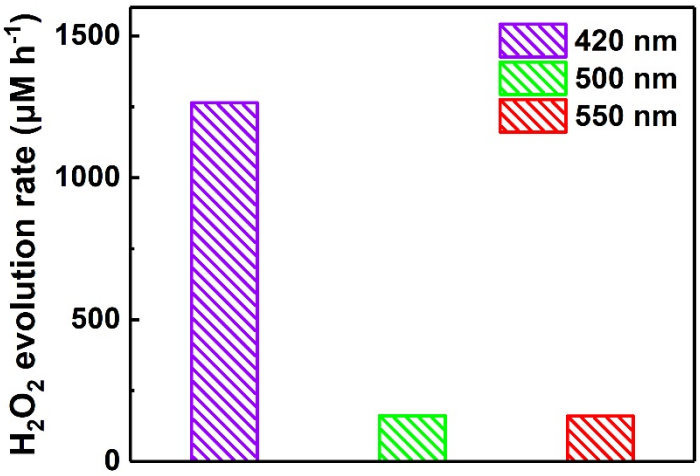

Figure S11. Histogram of H_2O_2 production for TCN/$NaI_{0.4}$ under 420nm, 500nm, 550nm light irradiation.

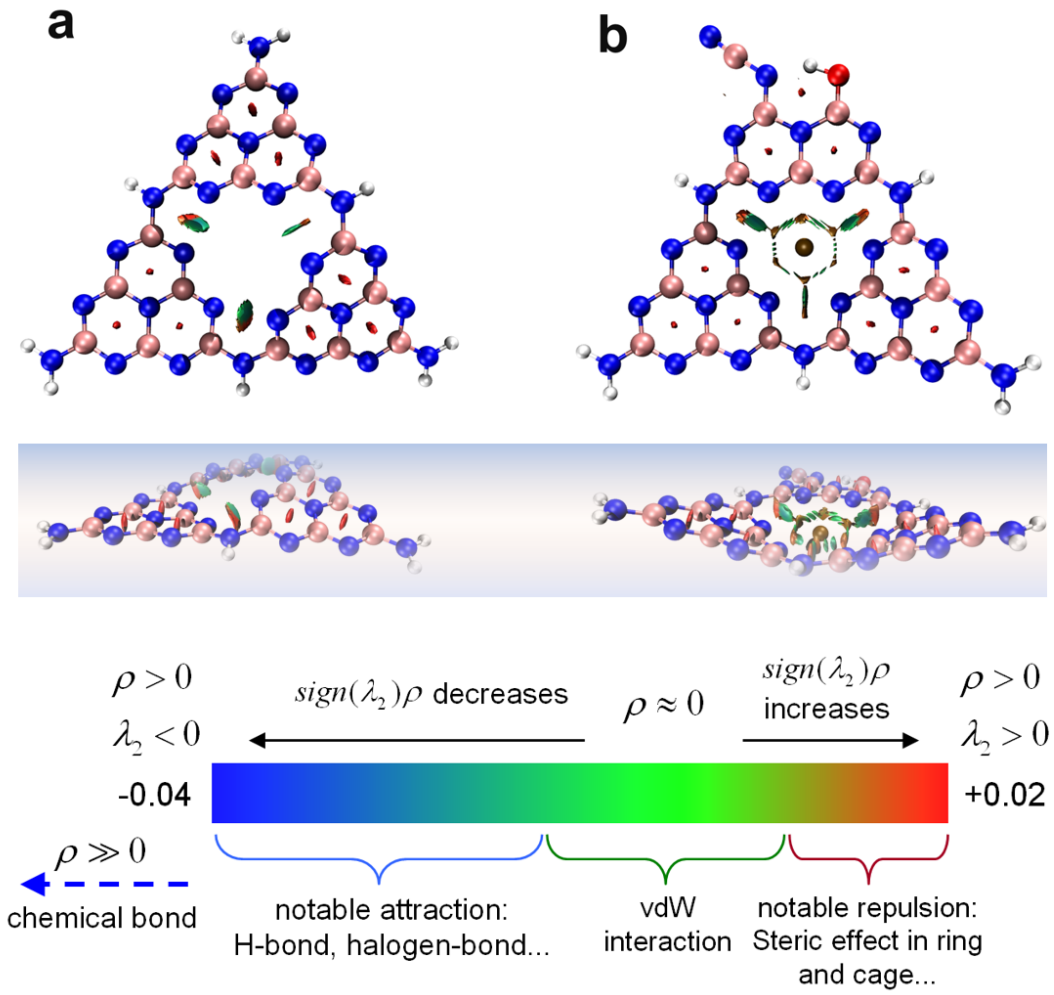

Figure S12. Isosurface map of IRI of pure BCN and TCN/NaI.

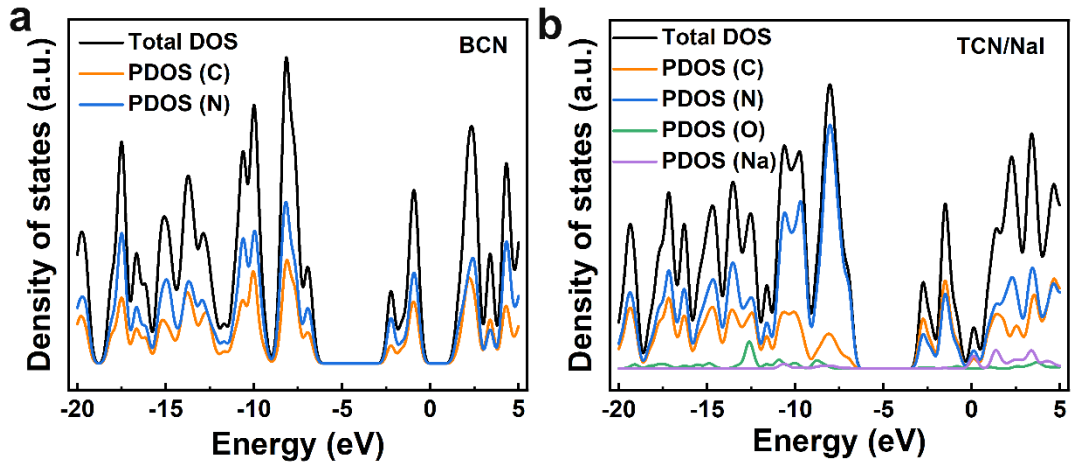

Figure S13. Total density of states (DOS) and partial density of states (PDOS) of pure BCN and TCN/NaI.

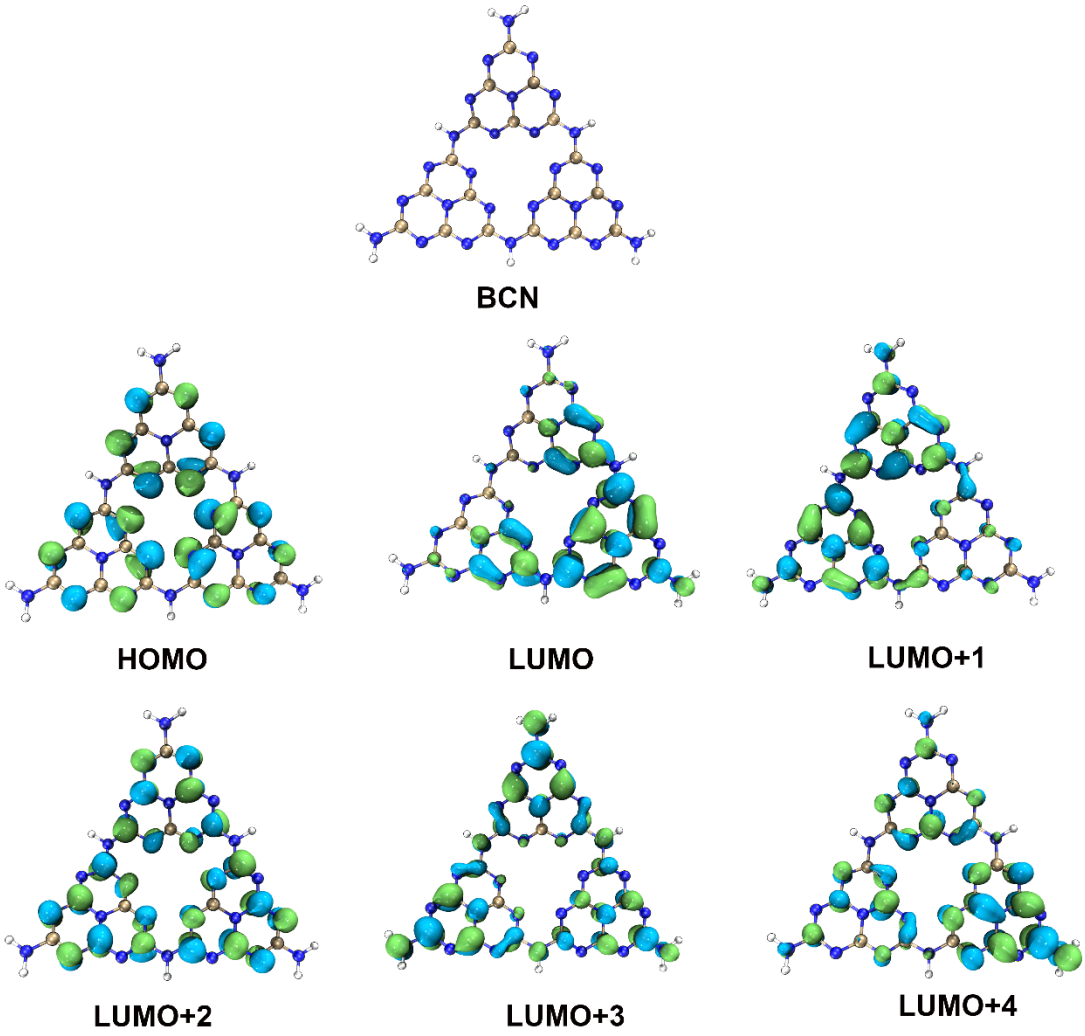

Figure S14. Electronic structure of the optimized HOMO and LUMO of pure BCN. Green and blue isosurfaces represent electron and hole distributions, respectively. The isosurface value is 0.003 e/Å^3.

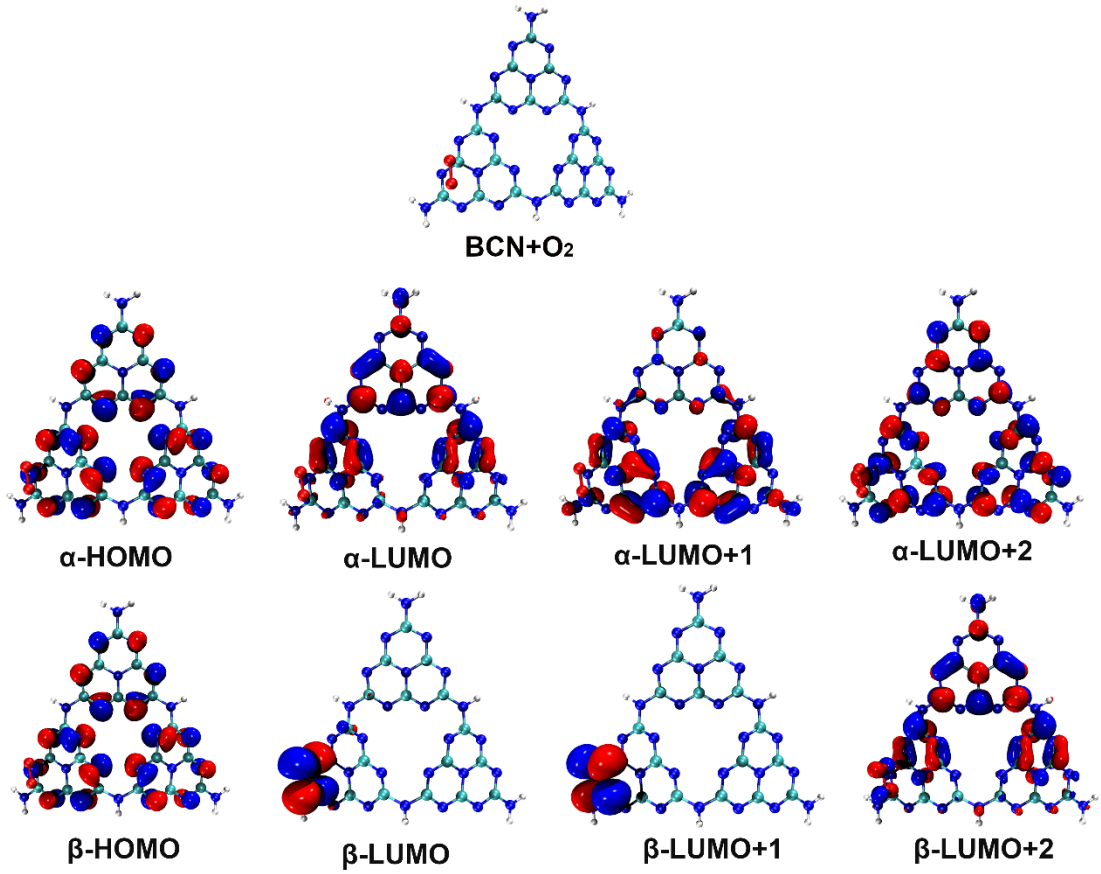

Figure S15. Electronic structure of the optimized HOMO and LUMO of O_2 adsorbed BCN. Red and blue isosurfaces represent electron and hole distributions, respectively. The isosurface value is 0.003 e/Å^3.

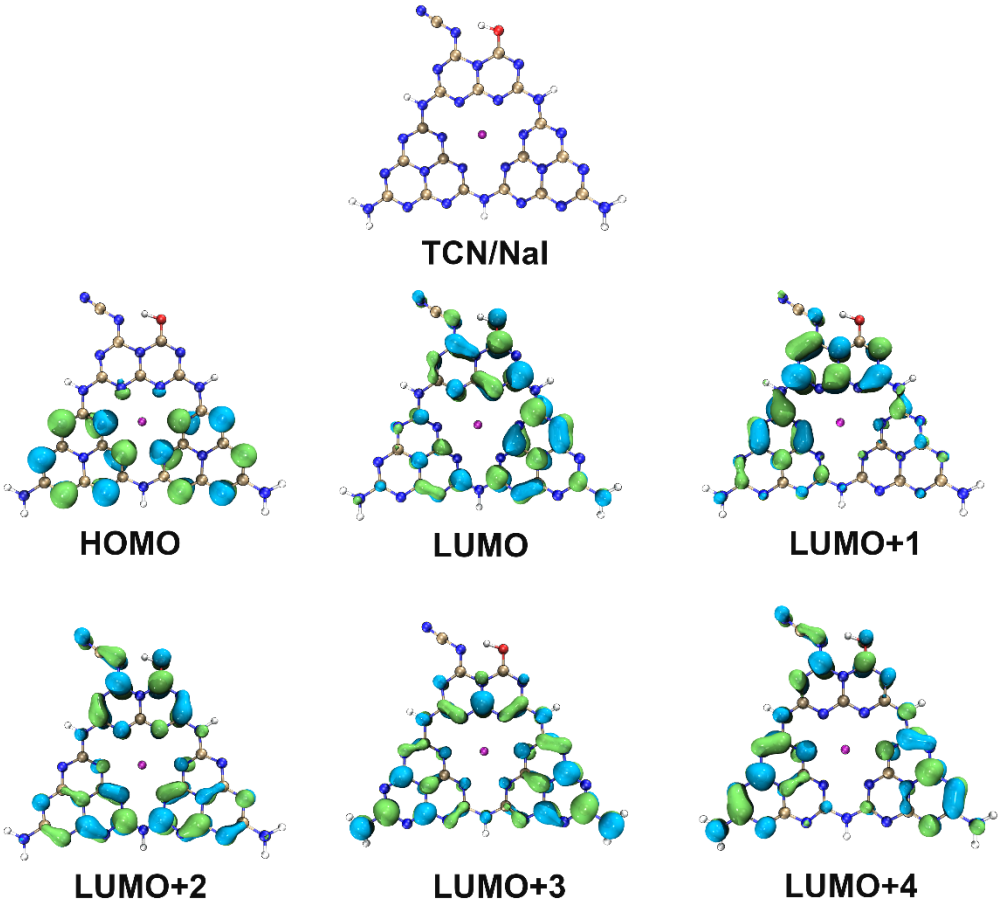

Figure S16. Electronic structure of the optimized HOMO and LUMO of TCN/NaI. Green and blue isosurfaces represent electron and hole distributions, respectively. The isosurface value is 0.003 e/Å^3.

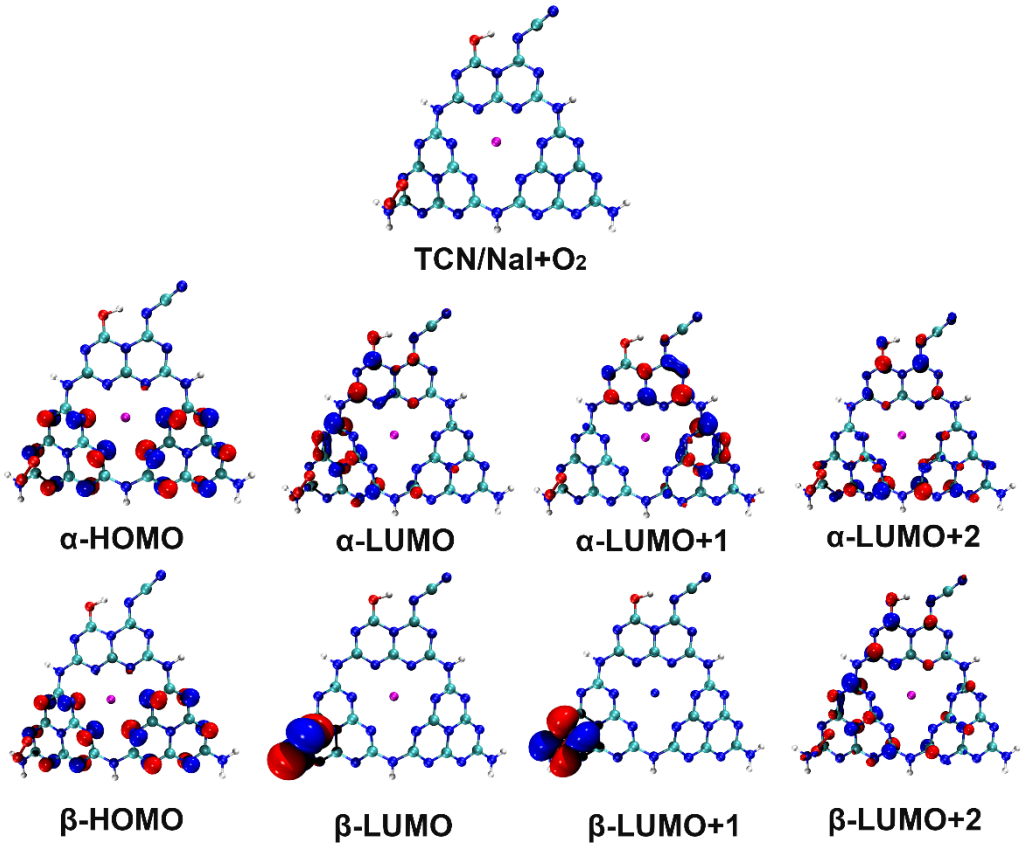

Figure S17. Electronic structure of the optimized HOMO and LUMO of O_2 adsorbed TCN/NaI. Red and blue isosurfaces represent electron and hole distributions, respectively. The isosurface value is 0.003 e/Å^3.

References

1 C. Adamo, V. Barone, *J. Chem. Phys.* 1999, **110**, 6158-6170.

2 S. Grimme, S. Ehrlich, L. Goerigk, *J. Comput. Chem.* 2011, **32**, 1456-1465.

3 S. Grimme, J. Antony, S. Ehrlich, H. Krieg, *J. Chem. Phys.* 2010, **132**, 154104-154122.

4 R. Ditchfield, W. J. Hehre, J. A. Pople, *J. Chem. Phys.* 1971, **54**, 724-728.

5 M. J. Frisch, G. W. Trucks, H. B. Schlegel, G. E. Scuseria, M. A. Robb, J. R. Cheeseman, G. Scalmani, V. Barone, G. A. Petersson, H. Nakatsuji, Gaussian 16, Revision C.01. Fox, Gaussian, Inc., Wallingford CT (2019).

6 A. V. Marenich, C. J. Cramer, D. G. Truhlar, *J. Phys. Chem. B* 2009, **113**, 6378-6396.

7 F. Weigend, R. Ahlrichs, *Phys. Chem. Chem. Phys.* 2005, **7**, 3297-3305.

8 P. W. Ayers, R. G. Parr, *J. Am. Chem. Soc.* 2000, **122**, 2010-2018.

9 P. Fuentealba, P. Pérez, R. Contreras, *J. Chem. Phys.* 2000, **113**, 2544-2551.

10 T. Lu, Q. Chen, *Chemistry-Methods,* 2021, **1**, 231-239.

11 Z. Liu, T. Lu, Q. Chen, *Carbon* 2020, **165**, 461-467.

12 T. Lu, F. Chen, *J. Comput. Chem.* 2012, **33**, 580-592.

13 W. Humphrey, A. Dalke, K. Schulten, *J. Molec. Graphics.* 1996, **14**, 33-38.

14 L. Goerigk, S. Grimme, *J. Chem. Theor. Comput.* 2010, **7**, 291-309.